Reverse Electron Transfer Completes the Catalytic Cycle in a 2,3,5-Trifluorotyrosine-Substituted Ribonucleotide Reductase

Kanchana R. Ravichandran,[†] Ellen C. Minnihan,[†,∥] Yifeng Wei,[†] Daniel G. Nocera,[§] and JoAnne Stubbe*,[†,‡]

[†]Department of Chemistry and [‡]Department of Biology, Massachusetts Institute of Technology, 77 Massachusetts Avenue, Cambridge, Massachusetts 02139, United States

[§]Department of Chemistry and Chemical Biology, Harvard University, 12 Oxford Street, Cambridge, Massachusetts 02138, United States

Ⓢ Supporting Information

ABSTRACT: *Escherichia coli* class Ia ribonucleotide reductase is composed of two subunits (α and β), which form an $\alpha2\beta2$ complex that catalyzes the conversion of nucleoside 5′-diphosphates to deoxynucleotides (dNDPs). $\beta2$ contains the essential tyrosyl radical ($Y_{122}^{\bullet}$) that generates a thiyl radical ($C_{439}^{\bullet}$) in $\alpha2$ where dNDPs are made. This oxidation occurs over 35 Å through a pathway of amino acid radical intermediates ($Y_{122} \rightarrow [W_{48}] \rightarrow Y_{356}$ in $\beta2$ to $Y_{731} \rightarrow Y_{730} \rightarrow C_{439}$ in $\alpha2$). However, chemistry is preceded by a slow protein conformational change(s) that prevents observation of these intermediates. 2,3,5-Trifluorotyrosine site-specifically inserted at position 122 of $\beta2$ ($F_3Y^{\bullet}$-$\beta2$) perturbs its conformation and the driving force for radical propagation, while maintaining catalytic activity (1.7 s^{-1}). Rapid freeze−quench electron paramagnetic resonance spectroscopy and rapid chemical-quench analysis of the $F_3Y^{\bullet}$-$\beta2$, $\alpha2$, CDP, and ATP (effector) reaction show generation of 0.5 equiv of $Y_{356}^{\bullet}$ and 0.5 equiv of dCDP, both at 30 s^{-1}. In the absence of an external reducing system, $Y_{356}^{\bullet}$ reduction occurs concomitant with F_3Y reoxidation (0.4 s^{-1}) and subsequent to oxidation of all $\alpha2$s. In the presence of a reducing system, a burst of dCDP (0.4 equiv at 22 s^{-1}) is observed prior to steady-state turnover (1.7 s^{-1}). The $[Y_{356}^{\bullet}]$ does not change, consistent with rate-limiting F_3Y reoxidation. The data support a mechanism where $Y_{122}^{\bullet}$ is reduced and reoxidized on each turnover and demonstrate for the first time the ability of a pathway radical in an active $\alpha2\beta2$ complex to complete the catalytic cycle.
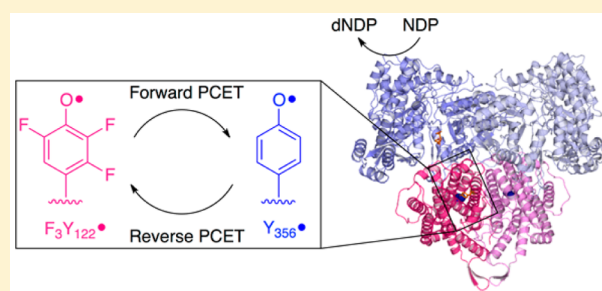
INTRODUCTION

Ribonucleotide reductases (RNRs) catalyze the formation of deoxynucleotides from their corresponding ribonucleotides (Scheme 1) in almost all organisms; allosteric regulation of substrate specificity and activity contributes to fidelity of both DNA replication and repair.[1,2] The class Ia RNRs contain two homodimeric subunits, $\alpha2$ and $\beta2$, which form an active $\alpha2\beta2$ complex in the case of the *E. coli* enzyme.[3] The $\beta2$ subunit houses a diferric-tyrosyl radical ($Y_{122}^{\bullet}$) cofactor that reversibly

oxidizes C_{439} in the active site of $\alpha2$ to a thiyl radical.[4,5] The $C_{439}^{\bullet}$ initiates nucleotide reduction by H atom abstraction from the 3′ position of the substrate (Scheme 1).[6,7] On the basis of *in silico* docking of the individual X-ray structures of $\alpha2$ and $\beta2$,[8,9] the distance between $Y_{122}^{\bullet}$ and C_{439} is estimated to be >35 Å. This radical transport (RT) process occurs through a specific pathway that involves at least three transient aromatic amino acid radical intermediates (proton-coupled electron transfer or PCET through $Y_{122}^{\bullet} \rightarrow [W_{48}] \rightarrow Y_{356}$ in $\beta2$ to $Y_{731} \rightarrow Y_{730} \rightarrow C_{439}$ in $\alpha2$, Figure 1).[9,10] During turnover of wild-type (wt) RNR, only the resting state $Y_{122}^{\bullet}$ is observed. In this paper, we describe the perturbation of PCET kinetics by site-specific incorporation of 2,3,5-trifluorotyrosine (F_3Y) at position 122 in $\beta2$ resulting in accumulation of a pathway tyrosyl radical intermediate ($Y_{356}^{\bullet}$) that is kinetically and chemically competent to complete the catalytic cycle of RNR.

In wt RNR, PCET steps are preceded by a rate-limiting protein conformational change(s) (5−10 s^{-1}) that occur(s) upon association of $\alpha2$, $\beta2$, substrate (S, CDP), and allosteric
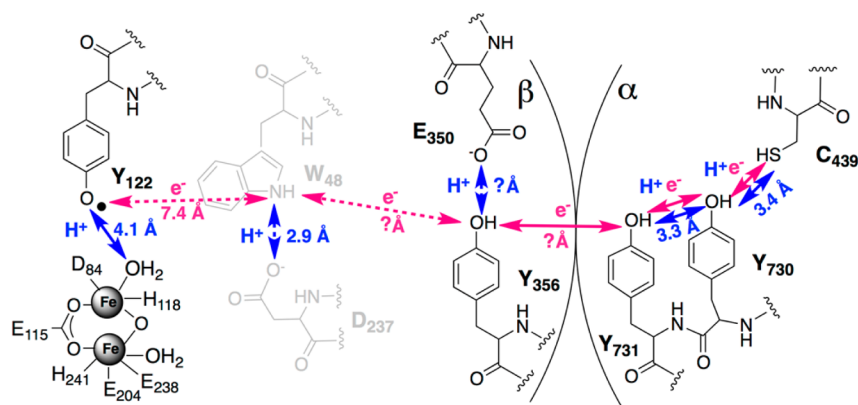
Scheme 1. Reaction Catalyzed by RNR[a]
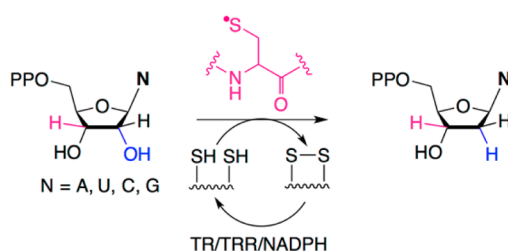
[a]Turnover requires reducing equivalents which are provided by a pair of cysteines in the active site of the enzyme.

14387

Figure 1. Proposed PCET pathway in *E. coli* class Ia RNR.[10] The pink and blue arrows indicate the movement of electrons and protons through conserved aromatic amino acids (Y_{356} in $\beta2$ and Y_{731} and Y_{730} in $\alpha2$). W_{48} and its putative proton acceptor D_{237} are shown in gray, as there is no evidence for their participation in RT. The positions of Y_{356} and E_{350} are unknown, as these residues are disordered in all crystal structures of $\beta2$.

effector (E, ATP).[11] Forward RT steps, active site chemistry, and reverse RT steps occur on a much more rapid time scale than the protein conformational change(s) preventing observation of radical intermediates either during steady-state turnover or using rapid kinetic methods.[11] An approach adopted by our lab has been to change the rate-limiting step of the reaction by site-specifically incorporating tyrosine analogues with perturbed pK_a's and reduction potentials in an effort to accumulate and characterize the proposed radical intermediates (Figure 1). Previously, we described the insertion of 3-nitrotyrosine (NO_2Y) at residue 122 in $\beta2$.[12] The reaction of $NO_2Y^\bullet$-$\beta2$, $\alpha2$, CDP, and ATP rapidly generates 0.5 equiv of $Y_{356}^\bullet$ and dCDP (>100 s^{-1}). We have proposed that this stoichiometry is a consequence of half-sites reactivity in RNR where only 50% of $Y_{122}^\bullet$ in the $\alpha2\beta2$ complex reacts at a time.[13−17] We have recently shown that, upon radical initiation in wt RNR, a proton is transferred from a water molecule on the diferric cluster to generate the corresponding Y_{122} phenol (Figure 1).[18] In contrast, use of $NO_2Y^\bullet$-$\beta2$ to initiate RT uncouples this proton transfer (PT) and electron transfer (ET); the conjugate base NO_2Y^- is generated instead of the anticipated phenol NO_2Y. Furthermore, $Y_{356}^\bullet$ generated during reverse RT is unable to reoxidize NO_2Y^-, and thus, this mutant could only perform a single turnover.[12] This prevented us from establishing the chemical competence of $Y_{356}^\bullet$ to complete the catalytic cycle and determining if it is a true intermediate on the PCET pathway.

In an attempt to engineer a smaller perturbation to the driving force, we inserted F_3Y at position 122 in $\beta2$ and investigated the reaction of $F_3Y^\bullet$-$\beta2$, $\alpha2$, CDP, and ATP.[19] Steady-state assays revealed that, unlike the $NO_2Y^\bullet$-$\beta2$ mutant, $F_3Y^\bullet$-$\beta2$ can catalyze multiple turnovers at 25% the steady-state wt activity. Hand-quench EPR experiments showed formation of a new tyrosyl radical, assigned to residue Y_{356} in $\beta2$ based on multiple lines of evidence. First, the new radical is observed when the redox inert F is inserted at position 731 but not at position 356.[19] Second, the 9 GHz EPR spectrum of the new radical is remarkably similar to that of the radical observed in the $NO_2Y^\bullet$-$\beta2$ studies.[12,19] In $NO_2Y^\bullet$-$\beta2$, pulsed electron−electron double resonance (PELDOR) spectroscopy experiments measured a distance of 30 Å between the new radical in one α/β pair and $NO_2Y^\bullet$ in the second α/β pair.[20] Similar experiments with other un-natural amino acids inserted at position 356 (either 3,4-dihydroxyphenylalanine[21] or 3-aminotyrosine[22]) provide an identical distance measurement (30 Å). In preliminary PELDOR experiments, a similar distance is also observed between $F_3Y^\bullet$ and the new

radical (Nick, Bennati, unpublished results). These data together support that the radical observed in $F_3Y^\bullet$-$\beta2$ is located at position 356. Studies with $NO_2Y^\bullet$-$\beta2$, however, have shown that while the predominant location of the radical is at position 356 (85−90%), $Y_{356}^\bullet$ is in equilibrium with $Y_{731}^\bullet$ and $Y_{730}^\bullet$ in $\alpha2$ (15−10%).[20] These initial studies laid the foundation for the work described herein and gave us an opportunity to investigate the importance of $Y_{356}^\bullet$ and reverse RT in an active RNR complex.

In this work, we carry out thorough kinetic analyses of the reaction of $F_3Y^\bullet$-$\beta2$, $\alpha2$, CDP, and ATP in the absence and presence of an external reducing system composed of thioredoxin (TR), thioredoxin reductase (TRR), and NADPH. Rapid freeze−quench (RFQ) EPR spectroscopy and rapid chemical-quench (RCQ) studies in the absence of a reducing system demonstrate that $Y_{356}^\bullet$ is kinetically and chemically competent; similar amounts of $Y_{356}^\bullet$ and dCDP are produced at similar rate constants. Furthermore, subsequent to complete oxidation of $\alpha2$, $Y_{356}^\bullet$ reduction occurs concomitant with F_3Y reoxidation. RCQ analysis in the presence of a reducing system shows a burst of dCDP prior to steady-state turnover suggesting that the rate-limiting step occurs after product formation. EPR studies detect no changes in $Y_{356}^\bullet$ concentration during steady-state turnover. Together, the data support the conclusion that reverse RT within $\beta2$ leading to regeneration of $F_3Y^\bullet$ is rate-limiting during steady-state turnover of $F_3Y^\bullet$-$\beta2$.

■ MATERIALS AND METHODS

Materials. (His)$_6$ wt-$\alpha2$ (specific activity of 2500 nmol/min/mg) was expressed from pET28a-*nrdA* and purified using our standard protocol.[23] Wt-$\alpha2$ was pre-reduced by the addition of DTT and hydroxyurea prior to use.[24] Tyrosine phenol lyase (TPL) was expressed and purified as described.[25] F_3Y was enzymatically synthesized from the corresponding phenol using TPL.[26] The pBAD-*nrdB*$_{122TAG}$ and pEVOL-F_nYRS-E3 plasmids were generated and isolated as described.[19] Apo F_3Y-$\beta2$ was expressed, purified, and reconstituted as detailed in the Supporting Information (SI). Yields of 10−15 mg of pure apo protein/g cell paste are routinely obtained. Reconstituted $F_3Y^\bullet$-$\beta2$ has a specific activity (750−1000 nmol/min/mg) that varies directly with the radical content (0.6−0.8 $F_3Y^\bullet$/$\beta2$). *E. coli* TR (40 U/mg) and TRR (1400 U/mg) were purified using established protocols.[27,28] [^{3}H] CDP was purchased from ViTrax (Placentia, CA). Hepes, MgSO$_4$, EDTA, 2XYT microbial medium, ampicillin (Amp), chloramphenicol (*Cm*), ATP, CDP, and carrier deoxycytidine (dC) were obtained from Sigma-Aldrich. Promega provided isopropyl β-D-1-thiogalactopyranoside (IPTG) and DTT. Calf alkaline phosphatase was purchased from Roche. Assay buffer consists of 50 mM Hepes pH 7.6, 15 mM MgSO$_4$, and 1 mM EDTA.

Reaction of F₃Y•-β2, wt-α2, CDP, and ATP Monitored by RFQ-EPR Spectroscopy. RFQ experiments were performed on an Update Instruments 1019 syringe ram unit and a model 715 Syringe Ram controller (ram speed 1.25−1.6 cm/s) equipped with a Lauda RM6 circulating water bath set at 5 or 25 °C. $F_3Y^\bullet$-β2 (0.4−0.8 $F_3Y^\bullet$/β2, 80 μM) and CDP (2 mM) in assay buffer was mixed on a rapid time scale (16 ms−15 s) with an equal volume of wt-α2 (80 μM) and ATP (6 mM) in assay buffer. The reaction was quenched in liquid isopentane (−140 °C), and the crystals were packed into EPR tubes for analysis by EPR spectroscopy. A packing factor of 0.60 ± 0.02 was determined for wt-β2. The reaction was additionally monitored on a longer time scale (20 s−2 min) by mixing all assay ingredients by hand (30 μM wt-α2, 30 μM $F_3Y^\bullet$-β2, 1 mM CDP, and 3 mM ATP) and quenching in liquid isopentane. EPR spectroscopy was performed at the Department of Chemistry Instrumentation Facility at MIT using wt-β2 (1.2 $Y^\bullet$/β2) as a standard. The concentration of $Y^\bullet$ in the wt-β2 standard was previously estimated using a Cu(II)SO₄ standard.[29] EPR spectra were recorded at 77 K on a Bruker EMX X-band spectrometer with a quartz finger dewar containing liquid N₂. The parameters were as follows: microwave frequency 9.45 GHz, power 30 μW, modulation amplitude 1.50 G, modulation frequency 100 kHz, time constant 5.12 ms, and scan time 41.93 s. From each composite spectrum, residual $F_3Y^\bullet$ was subtracted by aligning the radical's distinct features on the high- and low-field sides of the spectrum as previously reported (Figure S1).[19] The subtracted spectrum was reintegrated to quantitate the percentage of any observed pathway radical. The complete data sets at 5 and 25 °C were fit to eq 1:

$$y = A_1(1 - e^{-k_1 t}) + A_2(1 - e^{-k_2 t}) \tag{1}$$

where A_1 and A_2 are the amplitudes of the two phases and k_1 and k_2 are the observed rate constants.

Reaction of F₃Y•-β2, wt-α2, CDP, and ATP Monitored by the RCQ Method. RCQ experiments were performed on a KinTek RQF-3 instrument equipped with a Lauda RM6 circulating water bath set at 5 or 25 °C. Syringe A containing 20 μM wt-α2 and 6 mM ATP in assay buffer was mixed with an equal volume from syringe B containing 20 μM $F_3Y^\bullet$-β2 (0.85 $F_3Y^\bullet$/β2) and 1 mM [³H] CDP (22 000 cpm/nmol) in assay buffer. The reaction was aged for varying times (5 ms−100 s) and quenched with 2% HClO₄ in syringe C. The reaction was additionally monitored at >100 s by mixing the contents of the two syringes by hand, incubating the reaction mixture in a circulating water bath for the desired period of time, and manually quenching the reaction with 2% HClO₄. All samples were neutralized by the addition of 110−160 μL of 0.5 M KOH and worked up as described.[11,30] For the measurement of radioactive background from [³H] CDP, an equal volume of the contents of syringe B was mixed with assay buffer, followed by 2% HClO₄ and KOH. The reaction was also performed by hand (100 s at 5 or 25 °C) before and after the entire RCQ time course to account for any air oxidation of wt-α2. The 5 °C data set was fit to eq 1, and the 25 °C data set was fit to eq 2:

$$y = 0.50(1 - e^{-30t}) + A_2(1 - e^{-k_2 t}) + k_3 t \tag{2}$$

In eq 2, the first phase is fixed, A_2 and k_2 represent the amplitude and rate constant of the second phase, and k_3 represents the rate constant for the third phase.

Reaction of F₃Y•-β2, wt-α2, CDP, ATP, TR/TRR/NADPH Monitored by Hand-Quench EPR Spectroscopy. Reactions were performed in a total volume of 250 μL containing 10 μM wt-α2, 10 μM $F_3Y^\bullet$-β2 (0.6 $F_3Y^\bullet$/β2), 1 mM CDP, 3 mM ATP, 40 μM TR, 0.8 μM TRR, and 1 mM NADPH in assay buffer. Samples were incubated in a circulating water bath set at 5 °C and quenched for EPR analysis between 20 and 90 s in liquid isopentane (−140 °C). The reactions were also performed at 25 °C in a final volume of 250 μL containing 30 μM wt-α2, 10 μM $F_3Y^\bullet$-β2 (0.6 $F_3Y^\bullet$/β2), 2.5 mM CDP, 3 mM ATP, 80 μM TR, 1.6 μM TRR, and 2.5 mM NADPH.

Reaction of F₃Y•-β2, wt-α2, CDP, ATP, and TR/TRR/NADPH Monitored by the RCQ Method. The reaction was performed in an identical fashion to that described in the absence of a reducing system with minor modifications. For data collected at 5 °C, syringe A contained

20 μM wt-α2, 6 mM ATP, 80 μM TR, and 1.6 μM TRR in assay buffer, while syringe B contained 20 μM $F_3Y^\bullet$-β2 (0.6 $F_3Y^\bullet$/β2), 1 mM [³H] CDP (20 000 cpm/nmol), and 2 mM NADPH. For the 25 °C reaction, the amount of [³H] CDP in syringe B was increased to 2 mM. Samples were quenched and worked up as described earlier. The time courses of the reactions were fit to eq 3:

$$y = A(1 - e^{-k_1 t}) + k_2 t \tag{3}$$

Here A and k_1 are the amplitude and rate constant for the burst phase, respectively, and k_2 is the rate constant for the linear phase.

■ RESULTS

"Two or None" Radical Distribution and Half-Sites Reactivity in F₃Y•-β2. The diferric-$F_3Y^\bullet$ cofactor is self-assembled from apo F_3Y-β2 by the addition of Fe^{2+} and O_2 to produce ∼0.8 $F_3Y^\bullet$/β2 (SI), lower than the 1.2 $Y^\bullet$/wt-β2.[31] While the radical distribution in β2 has remained difficult to probe experimentally, evidence collected over the past few years supports that active β2 contains one $Y^\bullet$ in each monomer ("two or none", Figure 2A), suggesting that only ∼40% of β2 is active
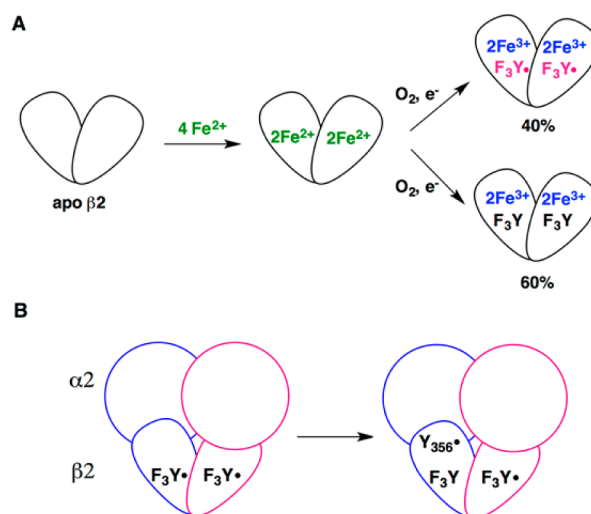
Figure 2. (A) "Two or none" model for radical distribution in $F_3Y^\bullet$-β2. The amounts of active (40%) and inactive β2 (60%) are shown for a sample containing 0.8 $F_3Y^\bullet$. The amount of radical in $F_3Y^\bullet$-β2 is lower than that typically seen in wt-β2 (1.2 $Y^\bullet$/β2).[31] (B) Half-sites reactivity in $F_3Y^\bullet$-β2. The total amount of $Y_{356}^\bullet$ that can accumulate on one turnover is 0.5 equiv/$F_3Y^\bullet$.

in our $F_3Y^\bullet$-β2 samples.[12,13,20−22,32,33] To provide support for this conclusion, we monitored the effect of $F_3Y^\bullet$ concentration on the amount of $Y_{356}^\bullet$ that accumulates. RFQ-EPR experiments were performed at 25 °C with $F_3Y^\bullet$-β2 containing 0.4 $F_3Y^\bullet$/β2 or 0.85 $F_3Y^\bullet$/β2, wt-α2, CDP, and ATP. The kinetic analysis of these studies is discussed subsequently, but the amount of $Y_{356}^\bullet$ is 0.43 and 0.5 equiv/$F_3Y^\bullet$, respectively (Table S1). This amount can be rationalized by the "two or none" radical distribution model (Figure 2A) as well as half-sites reactivity in RNR (Figure 2B); only one of the 2 $F_3Y^\bullet$ reacts at a time to generate $Y_{356}^\bullet$.[20−22]

Kinetics in the Absence of a Reducing System. *Kinetics of Formation and Disappearance of $Y_{356}^\bullet$ at 25 °C.* To assess if $Y_{356}^\bullet$ is formed faster than the turnover number of the enzyme (1.7 s^{-1}, Table 1), a RFQ-EPR experiment was performed in which wt-α2, $F_3Y^\bullet$-β2, CDP, and ATP were mixed rapidly (16 ms to 15 s). EPR analysis of each sample revealed a mixture of $F_3Y^\bullet$ and $Y_{356}^\bullet$, and spectral subtractions

Table 1. DeoxyCDP Formation Kinetics in the Absence and Presence of TR/TRR/NADPH[a]

$\beta 2$	T (°C)	R	first phase		second phase		total dC	
			k_1 (s^{-1})	A/radical	k_2 (s^{-1})	A/radical	dC/$\alpha 2$	dC/radical
F$_3$Y	25	N	30[b]	0.5[b]	0.5 (1)	2.9 (1)	2.8 (4)[c]	3.5 (3)[c]
F$_3$Y	25	Y	22 (9)	0.40 (5)	1.73 (4)			
F$_3$Y	5	N	3 (1)	0.3 (1)	0.08 (1)	2.9 (1)	2.7 (1)	3.4 (1)
F$_3$Y	5	Y	6 (3)	0.26 (5)	0.20 (1)			

[a]All experiments were performed with 10 μM wt-$\alpha 2$ and 10 μM F$_3$Y$^{\bullet}$-$\beta 2$. R notes the absence or presence of a reducing system. A represents the amplitude of each phase. [b]See description in main text and SI for more details regarding fitting. [c]Numbers reported reflect the total amount of dC generated within the first two phases. Product generated in the third phase is cytosine.
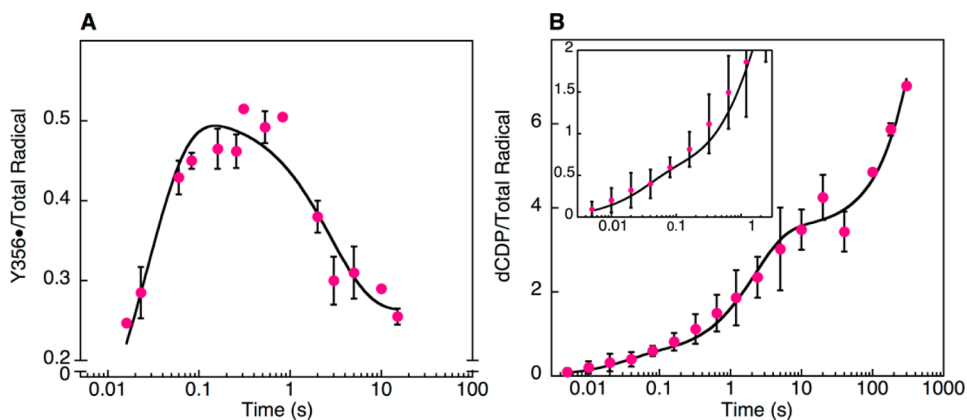
Figure 3. Reaction of F$_3$Y$^{\bullet}$-$\beta 2$, wt-$\alpha 2$, CDP, and ATP at 25 °C monitored by (A) RFQ-EPR spectroscopy and (B) the RCQ method. All data points represent the averages of two independent trials. Data were fit to a (A) two- or (B) three-phase model with the rate constants shown in Table 1. (B) The inset shows dCDP formation during the first 2 s of the reaction. The rate constants measured for Y$_{356}^{\bullet}$ formation and disappearance correlate with the fitted rate constants for dCDP formation in the first two phases.
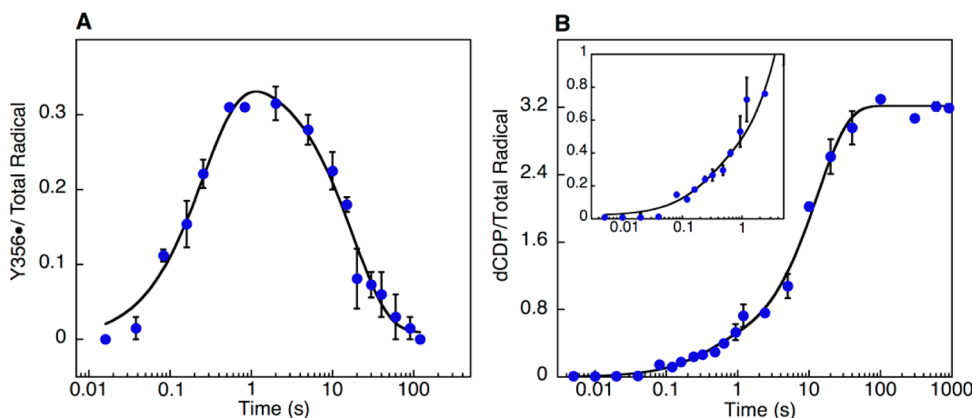
Figure 4. Reaction of F$_3$Y$^{\bullet}$-$\beta 2$, wt-$\alpha 2$, CDP, and ATP at 5 °C monitored by (A) RFQ-EPR spectroscopy and (B) the RCQ method. All data points represent the averages of two independent trials. Black lines represent biexponential fits to the data with the rate constants given in Table 1. (B) The inset shows dCDP formation during the first 5 s of the reaction. The rate constants measured for Y$_{356}^{\bullet}$ formation and disappearance are identical to the rate constants measured for dCDP formation.

were performed to quantitate the relative fraction of each radical. The unique hyperfine interactions associated with the fluorine nuclei facilitated spectral deconvolution (Figure S1).[19] The results of the experiment are shown in Figure 3A, and the data were fit to a biexponential equation. Rapid loss of 0.51 ± 0.02 equiv of F$_3$Y$^{\bullet}$ (not shown) concomitant with formation of identical amounts of Y$_{356}^{\bullet}$ occurs at 30 ± 5 s^{-1}. Subsequently, reduction of the pathway radical with k_{app} 0.4 ± 0.1 s^{-1} is accompanied by reformation of F$_3$Y$^{\bullet}$ with the same k_{app} (not shown). These data show for the first time, accumulation of a pathway radical (Y$_{356}^{\bullet}$) in an active RNR complex that can regenerate the stable radical at position 122 (F$_3$Y$^{\bullet}$). We note that

between 0.1 and 1 s, the concentration of Y$_{356}^{\bullet}$ varies minimally. As shown subsequently, F$_3$Y$^{\bullet}$-$\beta 2$ can make multiple dCDPs in the absence of a reducing system, and the reduction of Y$_{356}^{\bullet}$ and reoxidation of F$_3$Y are only visualized after the last turnover when all $\alpha 2$s are oxidized. Finally, regeneration of F$_3$Y$^{\bullet}$ is incomplete with only 0.25 equiv of Y$_{356}^{\bullet}$ reoxidizing F$_3$Y within 10 s.

Kinetics of Formation and Disappearance of Y$_{356}^{\bullet}$ at 5 °C. The rapid formation of Y$_{356}^{\bullet}$ at 25 °C resulted in generation of 0.25 equiv (50% of total Y$_{356}^{\bullet}$) prior to the first data point (16 ms, Figure 3A) prompting us to switch to lower temperatures to slow down the reaction. RFQ-EPR experiments were set up at 5 °C as described for 25 °C, and the results are shown in Figure 4A.

A k_{app} of 3.8 ± 0.5 s^{-1} was measured for formation of $Y_{356}^{\bullet}$ concomitant with loss of $F_3Y^{\bullet}$ (not shown). In contrast to our observation at 25 °C, only 0.32 ± 0.02 equiv of $Y_{356}^{\bullet}$ is formed at 5 °C reflecting temperature dependent changes in the rates of formation and decay of the pathway radical. Similar to our observation at 25 °C, the concentration of $Y_{356}^{\bullet}$ varies minimally between 0.8 and 5 s supporting the proposal that $F_3Y^{\bullet}$-β2 catalyzes multiple turnovers prior to visualization of reverse RT. Unlike in the 25 °C reaction, $Y_{356}^{\bullet}$ reduction at 5 °C is accompanied by complete reformation of $F_3Y^{\bullet}$ (0.3 equiv, 0.06 ± 0.01 s^{-1}) within ~40 s.

Kinetics and dCDP Formation with $F_3Y^{\bullet}$-β2 at 25 °C. Each dCDP generated by RNR is accompanied by the formation of a disulfide bond in the active site of an α monomer (Scheme 1, Figure 5, step A). Re-reduction of the active site
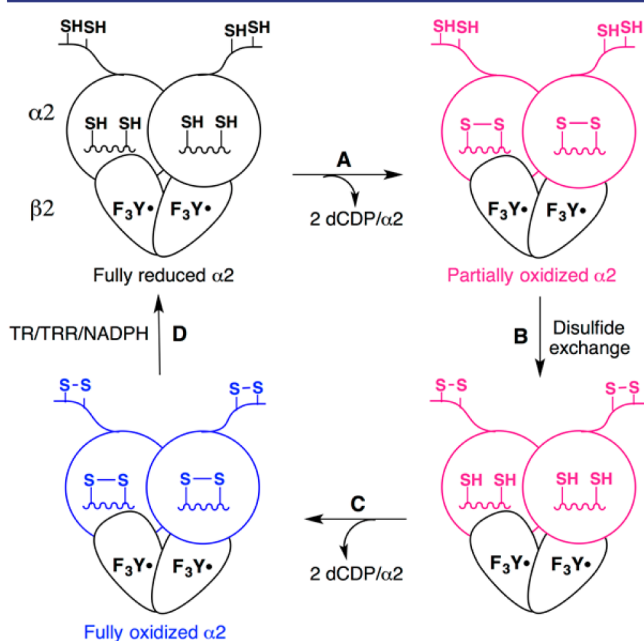
Figure 5. Amount of dCDP generated in the absence of a reducing system. A theoretical maximum of 4 dCDP/α2 can be produced; however, only 3 dCDP/α2 are routinely measured. The reaction mixture contains only 40% active $F_3Y^{\bullet}$-β2 (Figure 2A) supporting reorganization of active and inactive α2/$F_3Y^{\bullet}$-β2 complexes to oxidize all α2s.

disulfide by a C-terminal cysteine pair on each monomer (step B) facilitates an additional turnover (step C),[11] giving a theoretical maximum of 4 dCDP/α2 in the absence of TR/TRR/NADPH. In practice, only 3 dCDP/α2 are routinely measured with wt RNR due to partial oxidation of α2 (during purification and handling) and our inability to completely pre-reduce wt-α2 before an experiment.[11] Our kinetic experiments with $F_3Y^{\bullet}$-β2 contain 1:1 α2:$F_3Y^{\bullet}$-β2 with only 40% of active $F_3Y^{\bullet}$-β2 (Figure 2A). However, 3 dCDP/α2 are generated in the absence of a reducing system (Table 1) requiring that each $F_3Y^{\bullet}$ perform multiple turnovers (3.5 dCDP/$F_3Y^{\bullet}$, Table 1) to service all α2s.

To assess if $Y_{356}^{\bullet}$ is on-pathway, the kinetics of dCDP formation were determined. Wt-α2, $F_3Y^{\bullet}$-β2, [^{3}H] CDP, and ATP were mixed (5 ms to 300 s) and quenched rapidly with 2% HClO$_4$. CDP and dCDP were separated and analyzed by standard procedures,[11,30] and the results are shown in Figure 3B. The data are best described by eq 2 with a fixed first exponential phase, a variable second exponential phase, and a very slow third

linear phase. We initially attempted to fit the data with an exponential phase and a linear phase with poor results (Figure S2A). To obtain the fit shown in Figure 3B (black line), we fixed the amplitude and rate constant (k_1) of the first phase at 0.5 dCDP/$F_3Y^{\bullet}$ and 30 s^{-1}, respectively. Fixing this phase was required due to the scatter in the data at early time points. This scatter is a result of "two or none" and half-sites reactivity associated with RNR (Figure 2A,B). The [^{3}H] dCDP measured between 5 and 100 ms is close to the background measured with [^{3}H] CDP in the absence of α2. The range of choices considered for the amplitude and k_1 of this phase were based on the amplitude and rate constant measured for $Y_{356}^{\bullet}$ formation by RFQ-EPR (Figure 3A) and the results obtained in the presence of the reducing system (presented in the next section). The detailed description of data fitting using different parameters for the first kinetic phase is shown in Figure S2A–D. An additional experiment to justify the fixed first phase is shown in Figure S3.

Once the first phase was fixed using eq 2, we obtained an amplitude and rate constant (k_2) of 2.9 ± 0.1 dCDP/$F_3Y^{\bullet}$ and 0.5 ± 0.1 s^{-1}, respectively, for the second phase and a rate constant (k_3) of 0.012 ± 0.001 s^{-1} for the linear phase. This slow linear phase is associated with cytosine release and not dCDP formation. It occurs during the reaction of $F_3Y^{\bullet}$-β2 with oxidized α2 as shown in Scheme S1.[34] In a second manuscript, we show that the inability to monitor complete reverse RT at 25 °C (Figure 3A) is associated with reoxidation of Y_{356} (0.25 equiv) by $F_3Y^{\bullet}$-β2/oxidized α2.

The fit shown in Figure 3B suggests that the pathway radical is kinetically and chemically competent for nucleotide reduction at 25 °C. These data require that $Y_{356}^{\bullet}$ accumulates during reverse RT. k_2 for product formation correlates well with k_{app} for $Y_{356}^{\bullet}$ disappearance at this temperature (0.5 s^{-1} vs 0.4 s^{-1}, Figure 3A).

Kinetics and dCDP Formation with $F_3Y^{\bullet}$-β2 at 5 °C. The kinetics of dCDP formation were also measured at 5 °C, and the results are shown in Figure 4B. The data were fit to a bi-exponential equation providing amplitudes of 0.3 ± 0.1 dCDP/$F_3Y^{\bullet}$ and 2.9 ± 0.1 dCDP/$F_3Y^{\bullet}$ with k_1 and k_2 of 3 ± 1 s^{-1} and 0.08 ± 0.01 s^{-1}, respectively (Table 1). A_1 and k_1 for dCDP formation are very similar to the amplitude and rate constant measured for $Y_{356}^{\bullet}$ formation by RFQ-EPR spectroscopy at the same temperature (Figure 4A). These data suggest that $Y_{356}^{\bullet}$ is kinetically and chemically competent for dCDP formation and accumulates during reverse RT. Similar to our observations at 25 °C, k_2 of 0.08 s^{-1} for dCDP formation is similar to k_{app} of 0.06 s^{-1} for reoxidation of F_3Y by $Y_{356}^{\bullet}$ (Figure 4A).

The RCQ data were also analyzed relative to α2 to show that 2.7 ± 0.1 dCDPs/α2 are generated. DeoxyCDP formation was monitored for a total of 20 min, and in contrast to the 25 °C data, no third kinetic phase associated with cytosine was observed.

Kinetics in the Presence of a Reducing System. EPR Analysis of $Y_{356}^{\bullet}$ Concentration During Steady-State Turnover. The ability of $F_3Y^{\bullet}$-β2 to perform multiple turnovers in the absence of a reducing system (3.5 dCDP/$F_3Y^{\bullet}$, Table 1) and the observation of a plateau phase in the RFQ-EPR kinetic traces (Figures 3A and 4A) suggested that reverse RT is visualized subsequent to complete oxidation of α2. Thus, we predicted that the concentration of $Y_{356}^{\bullet}$ would vary minimally in the presence of the reducing system, TR/TRR/NADPH, as oxidized α2 is re-reduced. To test this prediction, $F_3Y^{\bullet}$-β2, wt-α2, CDP, and ATP were combined in the presence of TR/TRR/NADPH, and samples were quenched by hand in liquid isopentane between 20 and 90 s. In accordance with our
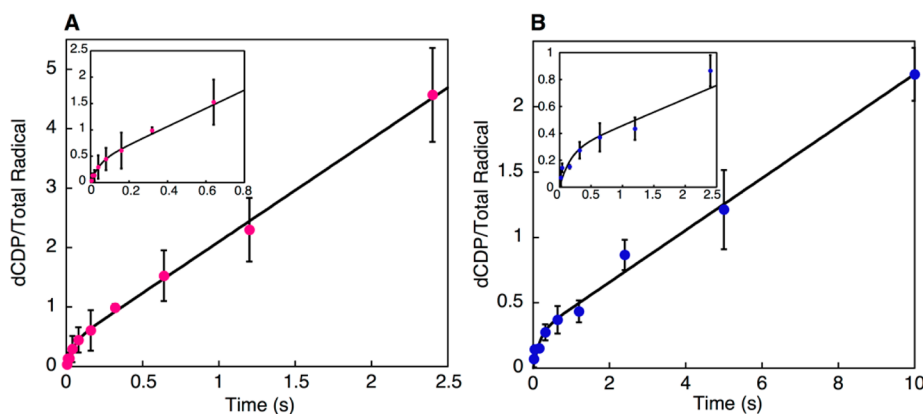
Figure 6. Kinetics of product formation in $F_3Y^\bullet$-$\beta 2$ in the presence of TR/TRR/NADPH at (A) 25 °C and (B) 5 °C. The averages of 2−4 separate trials are shown. Data were fit to a two-phase model with the rate constants given in Table 1. The insets show dCDP formation during the first (A) 0.8 s and (B) 2.5 s. The burst phase represents the very first turnover by an α/β pair. Reverse PCET regenerating $F_3Y^\bullet$ is rate-limiting during steady-state turnover.

Scheme 2. Kinetic Model for wt RNR in the Absence and Presence of a Reducing System[a]
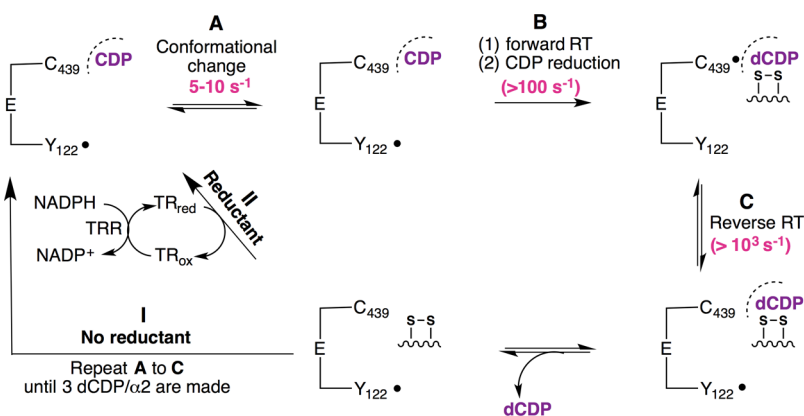
[a]The graphic shows only the key amino acids in the PCET pathway. Rate constants are shown for the reaction at 25 °C. $Y_{356}^\bullet$ cannot be visualized in wt RNR due to the rate-limiting conformational change(s). Figure adapted from ref 11.

prediction, the amount of $Y_{356}^\bullet$ does not change: 0.26 to 0.28 equiv/$F_3Y^\bullet$ at 5 °C and 0.40 to 0.46 equiv/$F_3Y^\bullet$ at 25 °C (Table S2). No reverse RT was visualized during the time frame of the reaction.

Kinetics of dCDP Formation at 5 and 25 °C. The observation of $Y_{356}^\bullet$ accumulation during reverse RT (Figures 3 and 4) in the absence of a reducing system and the lack of variation in [$Y_{356}^\bullet$] during steady-state turnover suggest that the rate-limiting step occurs subsequent to dCDP formation and $Y_{356}^\bullet$ reformation during reverse RT. This model predicts that RCQ experiments in the presence of the reducing system would show a burst of dCDP representing the first turnover followed by a linear phase for steady-state turnover. $F_3Y^\bullet$-$\beta 2$, wt-$\alpha 2$, [^{3}H]CDP, and ATP were mixed in the presence of TR/TRR/NADPH, and the reaction was monitored from 5 ms to 100 s. The results of the $F_3Y^\bullet$-$\beta 2$ experiments, at 5 and 25 °C, are shown in Figure 6 and summarized in Table 1.

As predicted, a burst of dCDP formation is observed at both temperatures (0.26 ± 0.05 dCDP/$F_3Y^\bullet$ at 6 ± 3 s^{-1} at 5 °C and 0.40 ± 0.05 dCDP/$F_3Y^\bullet$ at 22 ± 9 s^{-1} at 25 °C) followed by a linear phase (0.20 ± 0.01 s^{-1} at 5 °C and 1.73 ± 0.04 s^{-1} at 25 °C). The large uncertainties observed in these parameters are associated with low amounts of dCDP arising from the "two or none" model (Figure 2A) and half-sites reactivity (Figure 2B). Unfortunately, we are unable to increase protein concentration in

these experiments as studies with wt RNR have revealed kinetic complexities associated with the re-reduction process[11] and potentially quaternary structure interconversions.[35]

The observed rate constant and amplitude for the burst phase are within error similar to the parameters observed for $Y_{356}^\bullet$ formation (Figures 3A and 4A) and support our conclusion that $Y_{356}^\bullet$ is on-pathway for dCDP formation. These data also correlate well with the kinetics of the first phase measured in the absence of TR/TRR/NADPH (0.3 dCDP/$F_3Y^\bullet$ at 3 s^{-1} at 5 °C and 0.5 dCDP/$F_3Y^\bullet$ at 30 s^{-1} at 25 °C) supporting that k_1 in the absence of a reducing system and the burst phase in the presence of TR/TRR/NADPH report on the first turnover by one $\alpha/F_3Y^\bullet$-β pair in the $\alpha 2/F_3Y^\bullet$-$\beta 2$ complex (Figure 2B). Subsequent to dCDP formation and $Y_{356}^\bullet$ regeneration during reverse RT, reoxidation of F_3Y and re-reduction of oxidized $\alpha 2$ facilitate further turnovers. We argue subsequently that the rate-limiting step in $F_3Y^\bullet$-$\beta 2$ is reoxidation of F_3Y by $Y_{356}^\bullet$.

■ DISCUSSION

The rate-limiting protein conformational change(s) that gate(s) *E. coli* class Ia RNR turnover has precluded insight into the 35 Å forward RT, nucleotide reduction, and reverse RT processes. Our current model for wt RNR based on studies similar to those described herein for $F_3Y^\bullet$-$\beta 2$ is shown in Scheme 2.

Scheme 3. Kinetic Model for F$_3$Y$^\bullet$-β2 in the Absence and Presence of a Reducing System^a
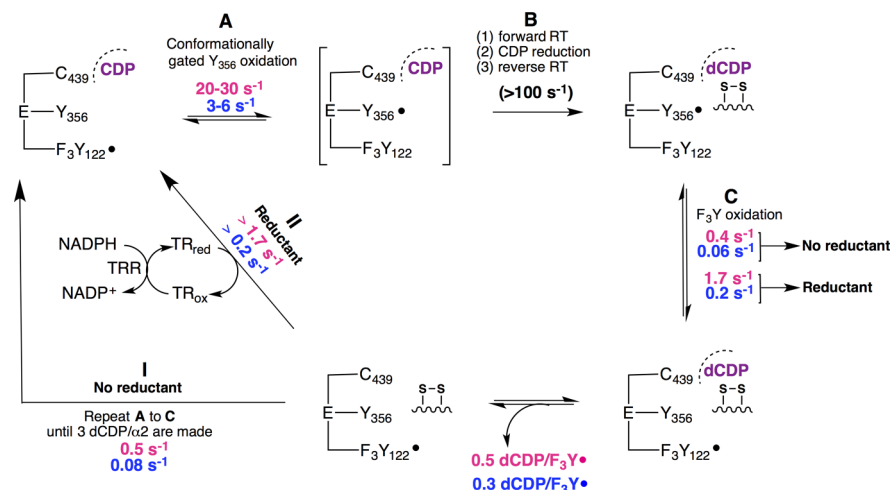
^{a}The figure represents a reductionist view of key amino acids in the PCET pathway. The rate constants for each step are shown in pink (25 °C), blue (5 °C), and black (both temperatures). It is not known if the first RT step involves PCET to generate the phenol (F$_3$Y), as in wt RNR or ET to generate the phenolate (F$_3$Y$^-$), as in NO$_2$Y$^\bullet$-β2.

Upon association of β2/α2/CDP/ATP, a conformational change(s) (5–10 s^{-1}, Scheme 2, step A) triggers rapid RT into α2 and nucleotide reduction (>100 s^{-1}, step B).[12,36] DeoxyCDP formation is rate-limited by the conformational change(s) and occurs at 5–10 s^{-1} as measured by RCQ methods reported previously[11] and reproduced here under the same conditions utilized for the F$_3$Y$^\bullet$-β2 studies (Figure S4). Subsequent to dCDP formation, reverse RT to regenerate Y$_{122}^\bullet$ is required to be downhill[12] and rapid (>10^3 s^{-1}, step C) as modeled by Ge et al.[11] to account for our inability to observe Y$_{122}^\bullet$ disappear and reappear during turnover (±TR/TRR/NADPH). The physical steps in wt RNR preclude detection of intermediates in these processes. Thus, studying the chemistry has required engineering specific perturbations to the system initially through site-directed mutagenesis[37−40] and the use of mechanism-based inhibitors[34,41,42] and, more recently, with site-specific incorporation of unnatural amino acids.[12,13,23,24] While with many of these approaches we were able to monitor the disappearance of Y$_{122}^\bullet$ concomitant with formation of new radicals, in none of these cases was the catalytic cycle of RNR completed, and no insight was obtained into reverse RT.

Our recent engineering of an orthogonal tRNA-synthetase tRNA pair that can incorporate di- and trifluorotyrosines (F$_n$Y, n = 2, 3) with a range of reduction potentials and pK_a's in RNR[19] allowed us to introduce a tunable thermodynamic perturbation of PCET kinetics with minimal steric perturbations. F$_3$Y is predicted as ~10 mV harder to oxidize than Y,[17,43] assuming that the first step in forward RT involves PT from the water on the diferric cluster to F$_3$Y$^\bullet$ concomitant with ET from Y$_{356}$ to F$_3$Y$^\bullet$ (Figure 1). F$_3$Y$^\bullet$-β2 is capable of catalyzing multiple turnovers but allows detection of Y$_{356}^\bullet$ (±TR/TRR/NADPH) due to perturbed reverse RT kinetics. Our current model for F$_3$Y$^\bullet$-β2 turnover is shown in Scheme 3. The ability to accumulate Y$_{356}^\bullet$ in F$_3$Y$^\bullet$-β2 but not in wt RNR is directly related to the differences in the rate-limiting step in the two systems.

In our model, the F$_3$Y$^\bullet$-β2/wt-α2/CDP/ATP complex undergoes a conformational change prior to generation of Y$_{356}^\bullet$ in one α/β pair (Scheme 3, step A). The RFQ-EPR data reported in Figures 3A and 4A provide the rate constants for this step and suggest that F$_3$Y$^\bullet$-β2 perturbs the conformational gate relative to

the wt enzyme (20−30 vs 5−10 s^{-1}). We expect that forward RT into α and dCDP production (step B in Schemes 2 and 3) occur with similar rate constants to wt RNR (>100 s^{-1}).[12,36] DeoxyCDP formation is rate-limited by the slow, conformationally gated generation of Y$_{356}^\bullet$ during forward RT as measured by the first phase in the absence of a reducing system (Figures 3B and 4B) or the burst phase in the presence of TR/TRR/NADPH (Figure 6) in the RCQ studies. Subsequent to product formation, we propose that reverse RT to regenerate Y$_{356}^\bullet$ is fast[12] as modeled in wt RNR where reverse RT to regenerate Y$_{122}^\bullet$ is 10^3 s^{-1}. However, unlike in wt RNR, slow reoxidation of F$_3$Y (step C) rate-limits subsequent turnovers.

In the absence of a reducing system, the RFQ-EPR data (Figures 3A and 4A) provide the rate constants for step C. Upon regeneration of F$_3$Y$^\bullet$, β2 rapidly dissociates from a partially oxidized α2, associates with a second reduced α2 and cycles through steps A−C until all α2s are completely oxidized.[44] Y$_{356}^\bullet$ concentration does not vary significantly during this time as visualized by the plateaus in the RFQ-EPR kinetic traces (Figures 3A and 4A). The second phase of the RCQ studies described in Figures 3B and 4B provides the rate constants for turnover in the absence of TR/TRR/NADPH (Scheme 3, branch I). Altered reverse RT kinetics in F$_3$Y$^\bullet$-β2 allow us to observe for the first time the disappearance and reappearance of the radical at position 122 subsequent to complete oxidation of α2. The molecular bases for our ability to observe reverse RT are not well-understood but are likely related to the initiating step in the PCET process. In addition to perturbing the driving force for RT, the fluoro substitutions could alter the distance between the phenolic oxygen and the water on the diferric cluster, thus affecting PT between the two (Figure 1). F$_3$Y also perturbs the pK_a at position 122 compared to Y (solution pK_a 6.4 vs 10).[43] Depending on the pK_a of the water on the diferric cluster, the phenolate F$_3$Y$^-$ could be generated instead of the anticipated phenol F$_3$Y.

Additional insight into the differences between wt and F$_3$Y$^\bullet$-β2 catalysis is obtained from the amplitudes for dCDP formation in the absence of a reducing system (Table 1 and Figure S4). In the F$_3$Y$^\bullet$-β2 system, the first phase (0.5 dCDP/F$_3$Y$^\bullet$ at 25 °C) reports on the very first turnover by an α/β pair (Figure 2B),

while the second phase (2.9 dCDP/$F_3Y^\bullet$) reports on consumption of all remaining reduced $\alpha2$s, rate-limited by reverse RT. This result is distinct from our previous[11] and current observations for wt RNR (Figure S4) where two phases are also measured for dCDP formation. The first phase is presumed to report on the conformationally gated generation of 2 dCDPs by all $\alpha2$s (the experimental observation is 1.3 ± 0.2 dCDP/$\alpha2$, 6 ± 1 s^{-1}), and the second phase is interpreted to report on the generation of 2 additional dCDPs subsequent to re-reduction of the active site disulfide (the experimental observation is 1.6 ± 0.2 dCDP/$\alpha2$, 0.5 ± 0.1 s^{-1}). The variation in the amplitudes of the two phases between wt and $F_3Y^\bullet$-$\beta2$ is consistent with different rate-limiting steps in the two systems. However, in both cases the total number of dCDPs generated is the same: 3 dCDP/$\alpha2$ (Schemes 2 and 3, branch I).

The EPR and RCQ data collected in the presence of a reducing system also lend support to Scheme 3. In $F_3Y^\bullet$-$\beta2$, a burst of dCDP formation prior to steady-state turnover is observed. The amplitude of this phase (~0.5 dCDP/$F_3Y^\bullet$ at 25 °C) again reflects that turnover occurs only on one α/β pair prior to the rate-limiting step and is consistent with slow reverse RT. Upon regeneration of $F_3Y^\bullet$ after one turnover (Scheme 3, step C), re-reduction of oxidized $\alpha2$ by TR/TRR/NADPH resets the system for additional turnovers (branch II). $Y_{356}^\bullet$ under these conditions behaves in a similar fashion to $Y_{122}^\bullet$ in wt RNR; i.e., no changes in its concentration are detected during steady-state conditions (Table S2). Slow reoxidation of F_3Y followed by rapid re-reduction, forward RT, nucleotide reduction, and regeneration of $Y_{356}^\bullet$ (Scheme 3, steps A−C) precludes observation of its disappearance and reappearance. We interpret the linear phases in Figure 6A,B as representative of the rate constants for reverse RT in the presence of a reducing system (Scheme 3, step C) and the rate constant limits for re-reduction of oxidized $\alpha2$. Although we set a lower limit for re-reduction from our experiments, we note that the rate constant for this step must be relatively fast, $>5-10$ s^{-1}, to account for our inability to monitor changes in $Y_{356}^\bullet$ concentration.

A comparison of the burst phase for $F_3Y^\bullet$-$\beta2$ and that for wt RNR in the presence of TR/TRR/NADPH reveals distinct behavior in the two systems (Figure 6 and Figure S5).[11] Although the conformational change is rate-limiting for dCDP formation in wt RNR, we have previously noted that the rate-limiting step in the presence of a reducing system can switch to re-reduction of oxidized $\alpha2$ at the high protein concentrations required for RCQ studies (10 μM).[11] In wt RNR, this results in a conformationally gated burst of 2 dCDPs by all $\alpha2$s (the experimental observation is 1.9 ± 0.1, 9 ± 2 s^{-1}) prior to steady-state turnover (Figure S5).[11] The burst phase reflects oxidation of all $\alpha2$ active sites despite the presence of only 60% active wt-$\beta2$ (1.2 $Y^\bullet$/$\beta2$, Figure 2A) and does not represent a single turnover. In contrast to the wt system, we have isolated the very first turnover by an $\alpha2\beta2$ complex with $F_3Y^\bullet$-$\beta2$ due to rate-limiting reverse RT.

As a final point, the rate constant measured for dCDP formation in the presence of a reducing system is 3-fold faster that that measured in its absence (Scheme 3, branch I vs I). A similar variation has been previously noted for dCDP formation in the wt system.[11] It is possible that re-reduction of the active site disulfide by the C-terminal tail (Figure 5, step B) is reversible and only driven to completion when the TR/TRR/NADPH system is included in the assays. However, we currently cannot rule out other modes by which TR accelerates re-reduction of the $\alpha2$ active site.

CONCLUSIONS

Radical initiation in the class I RNRs is proposed to involve long-range PCET through three pathway tyrosines.[9,10,17] Using an engineered RNR system, we have observed one of the proposed intermediates and demonstrate for the very first time chemically competent reverse RT that completes the RNR catalytic cycle. We additionally obtained insight into radical stoichiometry within $\beta2$, half-sites reactivity, and the ability of $\beta2$ to act catalytically during turnover. This work highlights the utility of unnatural amino acids in engineering specific perturbations for the study of redox active tyrosine residues in proteins; F_3Y could facilitate understanding of a number of additional tyrosyl radical mediated metabolic processes.[45−48]

ASSOCIATED CONTENT

$\textcircled{S}$ Supporting Information

The Supporting Information is available free of charge on the ACS Publications website at DOI: 10.1021/jacs.5b09189.

> Detailed experimental procedures, tables, figures, and scheme of cytosine release from CDP (PDF)

AUTHOR INFORMATION

Corresponding Author
*stubbe@mit.edu

Present Address
‖Merck Research Laboratories, 33 Avenue Louis Pasteur, Boston, MA 02115, United States.

Notes
The authors declare no competing financial interest.

ACKNOWLEDGMENTS

REFERENCES

(1) Stubbe, J.; van der Donk, W. A. *Chem. Rev.* **1998**, *98*, 705−62.
(2) Jordan, A.; Reichard, P. *Annu. Rev. Biochem.* **1998**, *67*, 71−98.
(3) Brown, N. C.; Canellakis, Z. N.; Lundin, B.; Reichard, P.; Thelander, L. *Eur. J. Biochem.* **1969**, *9*, 561−73.
(4) Licht, S.; Gerfen, G. J.; Stubbe, J. *Science* **1996**, *271*, 477−81.
(5) Stubbe, J. *Proc. Natl. Acad. Sci. U. S. A.* **1998**, *95*, 2723−4.
(6) Licht, S.; Stubbe, J. *Compr. Nat. Prod. Chem.* **1999**, *5*, 163−203.
(7) Stubbe, J.; Ackles, D. *J. Biol. Chem.* **1980**, *255*, 8027−30.
(8) Nordlund, P.; Sjöberg, B. M.; Eklund, H. *Nature* **1990**, *345*, 593−8.
(9) Uhlin, U.; Eklund, H. *Nature* **1994**, *370*, 533−9.
(10) Stubbe, J.; Nocera, D. G.; Yee, C. S.; Chang, M. C. Y. *Chem. Rev.* **2003**, *103*, 2167−201.
(11) Ge, J.; Yu, G.; Ator, M. A.; Stubbe, J. *Biochemistry* **2003**, *42*, 10071−83.
(12) Yokoyama, K.; Uhlin, U.; Stubbe, J. *J. Am. Chem. Soc.* **2010**, *132*, 15368−79.
(13) Seyedsayamdost, M. R.; Stubbe, J. *J. Am. Chem. Soc.* **2006**, *128*, 2522−3.
(14) Sjöberg, B. M.; Gräslund, A.; Eckstein, F. *J. Biol. Chem.* **1983**, *258*, 8060−7.
(15) Salowe, S.; Bollinger, J. M., Jr.; Ator, M.; Stubbe, J.; McCracken, J.; Peisach, J.; Samano, M. C.; Robins, M. J. *Biochemistry* **1993**, *32*, 12749−12760.
(16) Artin, E.; Wang, J.; Lohman, G. J.; Yokoyama, K.; Yu, G.; Griffin, R. G.; Bar, G.; Stubbe, J. *Biochemistry* **2009**, *48*, 11622−9.
(17) Minnihan, E. C.; Nocera, D. G.; Stubbe, J. *Acc. Chem. Res.* **2013**, *46*, 2524−35.

(18) Wörsdorfer, B.; Conner, D. A.; Yokoyama, K.; Livada, J.; Seyedsayamdost, M.; Jiang, W.; Silakov, A.; Stubbe, J.; Bollinger, J. M., Jr.; Krebs, C. *J. Am. Chem. Soc.* **2013**, *135*, 8585−93.

(19) Minnihan, E. C.; Young, D. D.; Schultz, P. G.; Stubbe, J. *J. Am. Chem. Soc.* **2011**, *133*, 15942−5.

(20) Yokoyama, K.; Smith, A. A.; Corzilius, B.; Griffin, R. G.; Stubbe, J. *J. Am. Chem. Soc.* **2011**, *133*, 18420−32.

(21) Seyedsayamdost, M. R.; Chan, C. T.; Mugnaini, V.; Stubbe, J.; Bennati, M. *J. Am. Chem. Soc.* **2007**, *129*, 15748−9.

(22) Minnihan, E. C. Ph.D. Dissertation, Massachusetts Institute of Technology, 2012.

(23) Minnihan, E. C.; Seyedsayamdost, M. R.; Uhlin, U.; Stubbe, J. *J. Am. Chem. Soc.* **2011**, *133*, 9430−40.

(24) Seyedsayamdost, M. R.; Xie, J.; Chan, C. T.; Schultz, P. G.; Stubbe, J. *J. Am. Chem. Soc.* **2007**, *129*, 15060−71.

(25) Chen, H.; Gollnick, P.; Phillips, R. S. *Eur. J. Biochem.* **1995**, *229*, 540−9.

(26) Seyedsayamdost, M. R.; Yee, C. S.; Stubbe, J. *Nat. Protoc.* **2007**, *2*, 1225−35.

(27) Chivers, P. T.; Prehoda, K. E.; Volkman, B. F.; Kim, B. M.; Markley, J. L.; Raines, R. T. *Biochemistry* **1997**, *36*, 14985−91.

(28) Russel, M.; Model, P. *J. Bacteriol.* **1985**, *163*, 238−242.

(29) Palmer, G. *Methods Enzymol.* **1967**, *10*, 594−610.

(30) Steeper, J. R.; Steuart, C. D. *Anal. Biochem.* **1970**, *34*, 123−30.

(31) Tong, W. H.; Chen, S.; Lloyd, S. G.; Edmondson, D. E.; Huynh, B. H.; Stubbe, J. *J. Am. Chem. Soc.* **1996**, *118*, 2107−8.

(32) Bennati, M.; Weber, A.; Antonic, J.; Perlstein, D. L.; Robblee, J. H.; Stubbe, J. *J. Am. Chem. Soc.* **2003**, *125*, 14988−9.

(33) Bennati, M.; Robblee, J. H.; Mugnaini, V.; Stubbe, J.; Freed, J. H.; Borbat, P. *J. Am. Chem. Soc.* **2005**, *127*, 15014−5.

(34) Ator, M. A.; Stubbe, J. *Biochemistry* **1985**, *24*, 7214−21.

(35) Ando, N.; Brignole, E. J.; Zimanyi, C. M.; Funk, M. A.; Yokoyama, K.; Asturias, F. J.; Stubbe, J.; Drennan, C. L. *Proc. Natl. Acad. Sci. U. S. A.* **2011**, *108*, 21046−51.

(36) Olshansky, L.; Pizano, A. A.; Wei, Y.; Stubbe, J.; Nocera, D. G. *J. Am. Chem. Soc.* **2014**, *136*, 16210−6.

(37) Lawrence, C. C.; Bennati, M.; Obias, H. V.; Bar, G.; Griffin, R. G.; Stubbe, J. *Proc. Natl. Acad. Sci. U. S. A.* **1999**, *96*, 8979−84.

(38) Mao, S. S.; Holler, T. P.; Yu, G. X.; Bollinger, J. M., Jr.; Booker, S.; Johnston, M. I.; Stubbe, J. *Biochemistry* **1992**, *31*, 9733−43.

(39) Persson, A. L.; Eriksson, M.; Katterle, B.; Pötsch, S.; Sahlin, M.; Sjöberg, B. M. *J. Biol. Chem.* **1997**, *272*, 31533−41.

(40) Kasrayan, A.; Persson, A. L.; Sahlin, M.; Sjöberg, B. M. *J. Biol. Chem.* **2002**, *277*, 5749−55.

(41) van der Donk, W. A.; Stubbe, J.; Gerfen, G. J.; Bellew, B. F.; Griffin, R. G. *J. Am. Chem. Soc.* **1995**, *117*, 8908−16.

(42) van der Donk, W. A.; Yu, G. X.; Pérez, L.; Sanchez, R. J.; Stubbe, J.; Samano, V.; Robins, M. J. *Biochemistry* **1998**, *37*, 6419−26.

(43) Seyedsayamdost, M. R.; Reece, S. Y.; Nocera, D. G.; Stubbe, J. *J. Am. Chem. Soc.* **2006**, *128*, 1569−79.

(44) Olshansky, L. Ph.D. Dissertation, Massachusetts Institute of Technology, 2015.

(45) Barry, B. A.; El-Deeb, M. K.; Sandusky, P. O.; Babcock, G. T. *J. Biol. Chem.* **1990**, *265*, 20139−43.

(46) Gupta, A.; Mukherjee, A.; Matsui, K.; Roth, J. P. *J. Am. Chem. Soc.* **2008**, *130*, 11274−5.

(47) Zhao, X.; Suarez, J.; Khajo, A.; Yu, S.; Metlitsky, L.; Magliozzo, R. S. *J. Am. Chem. Soc.* **2010**, *132*, 8268−9.

(48) Tsai, A. L.; Kulmacz, R. J. *Arch. Biochem. Biophys.* **2010**, *493*, 103−24.